Title
1 x N^2 wavelength-selective switch with two cross-scanning one-axis analog micromirror arrays in a 4-f optical system

Journal
Journal of Lightwave Technology, 24(2)

ISSN
0733-8724

Authors
Tsai, J C
Huang, STY
Hah, D
et al.

Publication Date
2006-02-01

Peer reviewed

$1 \times N^2$ Wavelength-Selective Switch With Two Cross-Scanning One-Axis Analog Micromirror Arrays in a $4 - f$ Optical System

Jui-che Tsai, Sophia Ting-Yu Huang, Dooyoung Hah, and Ming C. Wu, *Fellow, IEEE*

***Abstract*—A new high-port-count wavelength-selective switch (WSS) has been realized using two cross-scanning one-axis analog micromirror arrays in a $4 - f$ optical system. The number of output ports is increased from N to N^2, where N is the maximum linear port count limited by optical diffraction. Using surface-micromachined micromirrors with hidden vertical comb drives, large scan angles ($> \pm 5^\circ$ mechanical), low drive voltages (7 V), and high fill factors ($> 96.25\%$) are achieved for both scanning mirrors. Experimental results for WSS are demonstrated using both two-dimensional (2-D) array of discrete collimators and monolithic 2-D collimator array. A fiber-to-fiber insertion loss ranging from 6 to 18 dB and a switching time of < 700 μs have been achieved.**

***Index Terms*—Microelectromechanical devices, optical components, optical fiber switches, wavelength division multiplexing.**

I. Introduction

RECENT developments and advances in optical microelectromechanical systems (MEMS) play an important role in fiber communication networks. Several MEMS technologies have been successfully integrated into the telecommunication networks, such as two-dimensional (2-D) [1], [2] and three-dimensional (3-D) [3] cross connects. The use of MEMS techniques offers lower optical insertion loss, faster speed, higher extinction ratio, and the independence of wavelengths and polarizations.

Due to the wide deployment of wavelength division multiplexing (WDM) networks, devices capable of wavelength routing have become increasingly desirable. Wavelength-selective switches (WSSs) have attracted a great deal of attention due to their ability to route different wavelength channels independently. Liquid-crystal-based optical add/drop multiplexer (OADM) has been demonstrated [4]. It is basically a combination of a grating spectrometer with a spatial light modulator. Ford *et al.* proposed the first MEMS-based OADM using a digital micromirror array as the spatial light modulator [5]. This OADM is essentially a wavelength-selective 2×1 (add) switch concatenated with a 1×2 (drop) switch. A multiport WSS ($1 \times N$ WSS) can be realized by replacing the digital micromirrors with analog micromirrors and expanding the input/output fibers into a linear array. This is a useful network element because it can be used either as a versatile multiport add/drop multiplexer [6]–[14] or as a basic building block for $N \times N$ wavelength-selective cross connect (WSXC) [10], [12]. Several $1 \times N$ WSSs have been reported [6]–[14], and the maximum number of output ports reported to date is four, which is limited by optical diffraction. A larger port count (≥ 10) WSS is desired for high capacity networks.

By simply replacing the one-axis micromirror array with a linear array of two-axis scanners, a 2-D collimator array can be accommodated. This increases the port count from N to N^2. However, the designs and fabrication of high-fill-factor two-axis micromirror arrays are more challenging. Moreover, the control of two-axis scanner is more complicated. Previously, we proposed a novel $1 \times N^2$ WSS by combining two linear arrays of one-axis micromirrors with orthogonal rotation directions in a $4 - f$ optical imaging system [15]–[17]. This alternatively enables us to arrange the input/output fibers in a 2-D array. The 2-D beam steering mechanism for each WDM signal is then implemented by a pair of one-axis scanners with orthogonal scanning directions instead of a single two-axis scanner.

In this paper, we report on a comprehensive study on the scaling limit of WSSs. The tradeoff between port count and wavelength channel spacing will be discussed. A Gaussian beam model is used for the theoretical analysis. Experimentally, a 1×8 WSS with a channel spacing of 75 GHz using a 2-D array of discrete collimators is demonstrated. A 1×5 (scalable to 1×14) WSS with 200-GHz channel spacing, using a monolithic 2-D collimator array, is also shown. The fiber-to-fiber optical insertion loss is 6–18 dB, and the switching time is less than 700 μs.

II. Scaling Limit

A. Mirror Scan Angle

Fig. 1 shows the schematic of a $1 \times N$ WSS. The one-axis analog micromirror array is placed at the focal plane of a grating spectrometer. The WDM signals are spatially dispersed by the grating and focused onto the MEMS mirrors. They are then directed independently into any arbitrary output port in the

Manuscript received October 5, 2004; revised October 6, 2005. This work was supported by the Defense Advanced Research Projects Agency/Space and Naval Warfare Systems Command (DARPA/SPAWAR) under Contract N66001-00-C-8088.

J. Tsai is with the Graduate Institute of Electro-Optical Engineering and Department of Electrical Engineering, National Taiwan University, Taipei, Taiwan, R.O.C. (e-mail: jctsai@cc.ee.ntu.edu.tw).

S. T.-Y. Huang is with the Amuse Cosmetics Inc., Tustin, CA 92782 USA.

D. Hah is with the Department of Electrical and Computer Engineering, Louisiana State University (LSU), Baton Rouge, LA 70803 USA.

M. C. Wu is with the Department of Electrical Engineering and Computer Sciences, and Berkeley Sensor and Actuator Center (BSAC), University of California, Berkeley, CA 94720-1774 USA.

Digital Object Identifier 10.1109/JLT.2005.861915

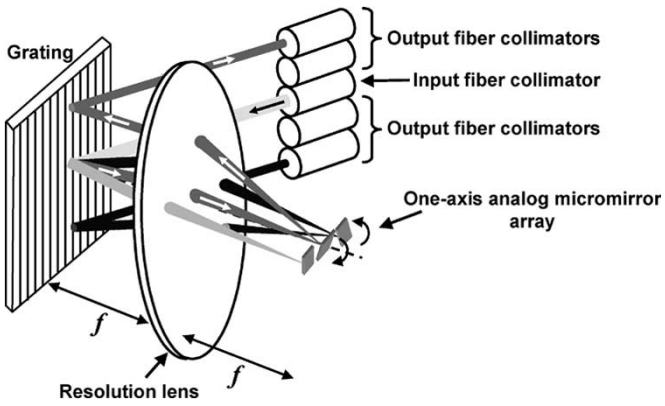

Fig. 1. Schematic diagram of the MEMS-based $1 \times N$ WSS.

linear fiber collimator array, depending on the mirror rotation angles. The mirror scan angle is one of the limiting factors of the scalability in the $1 \times N$ WSS. The number of output ports covered by the mirror scan angle is

$$N = \frac{f}{D_c} \tan(\theta_{\text{optical}})$$

where N, f, D_c, and $\theta_{optical}$ are the output port count, focal length of the resolution lens, distance between the collimator centers (pitch), and mirror optical scan angle, respectively. D_c can be expressed as $\zeta \times w_c$, where w_c is the Gaussian beam radius at collimators and ζ is a dimensionless factor. Generally, ζ is set to be ≥ 4 to ensure low crosstalk. The output port count increases with the mirror optical scan angle.

B. Optical Diffraction

Even though a larger scan angle is always preferred, it does not necessarily guarantee a larger number of output ports. Ultimately, the port count is limited by the effective optical aperture of the system, as illustrated in Fig. 2. Optical diffraction hence plays a fundamental role in the scalability of $1 \times N$ WSS.

The Gaussian beam radius on the MEMS mirror is

$$w_{\text{MEMS}} = \frac{1}{\xi} \Delta d_{\text{MEMS}} = \frac{\lambda f}{\pi w_c} = \frac{\zeta \lambda f}{\pi D_c}$$

where λ and Δd_{MEMS} are the optical wavelength of the WDM signal and the MEMS mirror pitch, respectively, and ξ is a dimensionless factor measuring how well the Gaussian mode is confined within the micromirror. The port count and the wavelength channel spacing are

$$N_{\text{spatial}} = \frac{D}{D_c} \quad \text{and} \quad \lambda_{\text{spacing}} = \frac{\Delta d_{\text{MEMS}}}{f \frac{\Delta\theta}{\Delta\lambda}}$$

where D and $\Delta\theta/\Delta\lambda$ are the effective aperture of the resolution lens and the grating dispersion, respectively. The ratio of port count (N_{spatial}) to wavelength channel spacing $(\lambda_{\text{spacing}})$ can be derived as

$$\frac{N_{\text{spatial}}}{\lambda_{\text{spacing}}} = \frac{\pi}{\zeta \xi \lambda} D \frac{\Delta\theta}{\Delta\lambda}.$$

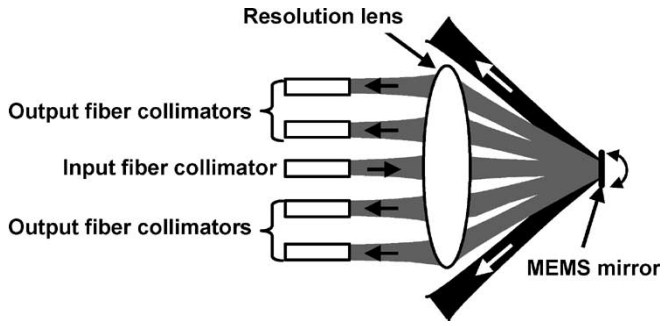

Fig. 2. Port count is fundamentally limited by the optical aperture of the resolution lens.

To achieve flat and wide passbands, normally ξ has to be ≥ 5.5 [18], [19]. It can be seen that the port count of $1 \times N$ WSS is fixed by the lens size and the grating dispersion for a given wavelength channel spacing. There is a tradeoff between port count and wavelength channel spacing. To increase the number of output ports without compromising the channel spacing requires more sophisticated optical design. Marom *et al.* [11] use anamorphic optics to compress the beam size in the direction orthogonal to the grating dispersion direction. This reduces the required size of the optical aperture, but the MEMS mirror dimension needs to be longer in the compression direction due to the larger focus spot size.

Alternatively, the port count can be increased from N to N^2 by using a 2-D collimator array. In this case, a 2-D beam steering mechanism is needed. The number of ports that can be allocated in the second (horizontal) direction is restricted by the optical aperture (D) as well as the physical extent of the micromirror array $K \times \Delta d_{\text{MEMS}}$, where K is the number of wavelength channels. It can be expressed as $(D - K \times \Delta d_{\text{MEMS}})/D_c$. Given a fixed grating dispersion $(\Delta\theta/\Delta\lambda)$ and the desired channel number (K) and spacing $(\lambda_{\text{spacing}})$, the spread of the micromirror array can be shrunk by reducing the mirror pitch (Δd_{MEMS}) and the focal length (f) proportionally. This pushes the port count in the horizontal direction closer toward the extreme of D/D_c without compromising the channel number and spacing. The reduction of the focal length leads to a larger required mirror scan angle and a smaller F# of the lens, both of which are in practice the limiting factors when pushing the horizontal port count toward D/D_c.

III. $1 \times N^2$ WSS

The schematic of the $1 \times N^2$ WSS is shown in Fig. 3(a). Two resolution lenses are arranged in a $4 - f$ confocal configuration to image the first micromirror array in plane A to the second micromirror array in plane B. The grating is inserted between the lenses in the upper half of the system. The axial position of the grating is adjusted such that the projected light spot from the input port is located at the common focus of the two lenses. The $4 - f$ configuration ensures that the optical beam focused on any mirror in the first array is always directed to the corresponding mirror in the second array, and vice versa, irrespective of the tilting angle of the mirrors. Thus, each wavelength is steered by two micromirrors in orthogonal scanning directions and directed toward the desired output fiber in the 2-D array.

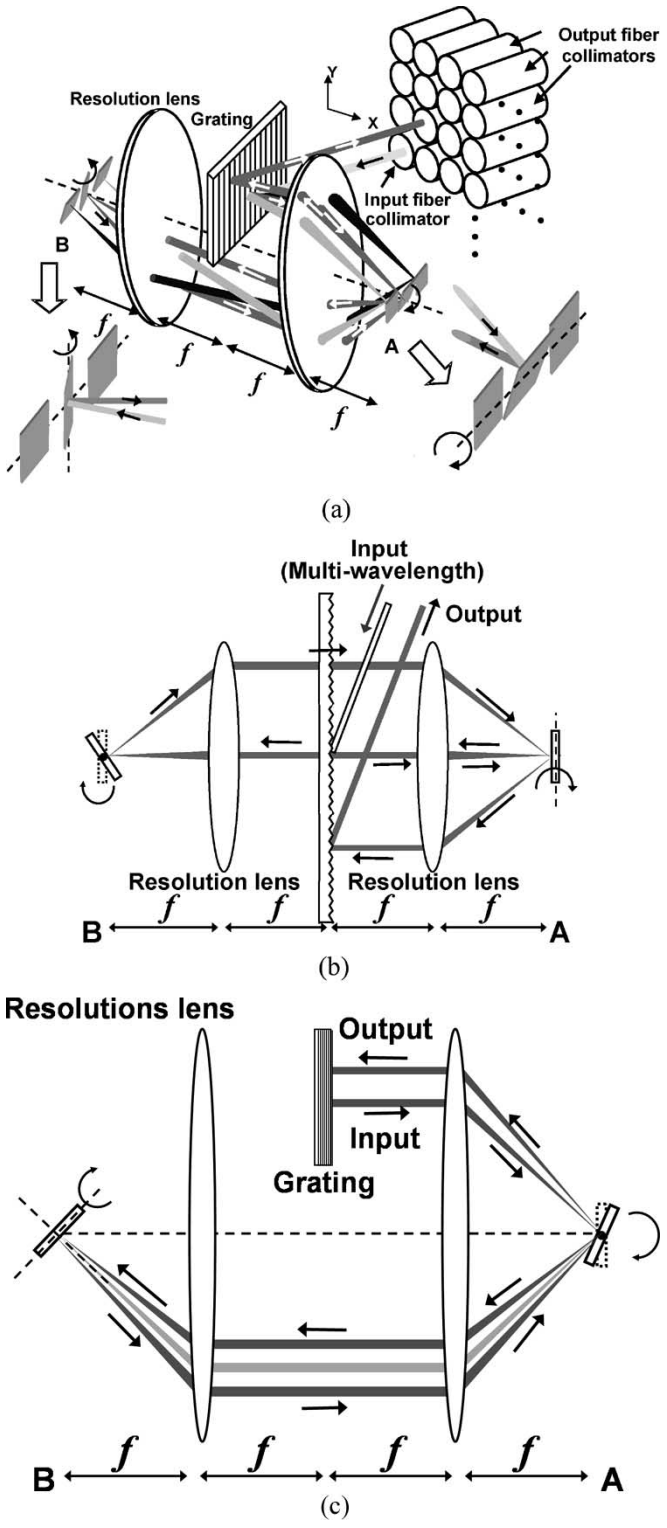

Fig. 3. (a) Schematic setup of the $1 \times N^2$ WSS. The two orthogonally scanning micromirror arrays enable the fibers to be arranged in two dimensions, which increases the output port from N to N^2. (b) Top view of the $1 \times N^2$ WSS. (c) Side view of the $1 \times N^2$ WSS.

Another benefit of this $4 - f$ configuration is that the laser beam passes through the first array twice. This doubles the deflection of the laser beam in the vertical direction. Therefore, more spatial channels can be supported. Fig. 3(b) and (c) show the top and side views of the $1 \times N^2$ WSS, respectively.

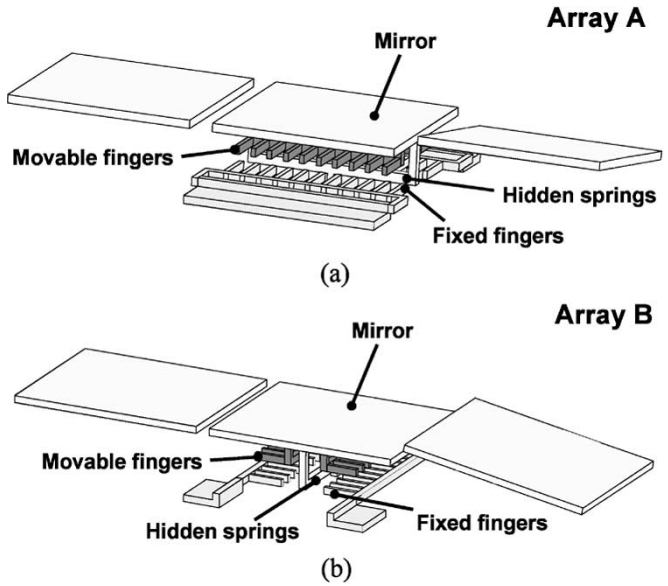

Fig. 4. Schematics of the analog micromirror arrays with hidden vertical comb-drive actuators. The scan directions of the mirrors are (a) perpendicular to and (b) in parallel with the array directions.

IV. Analog Micromirror Arrays

Fig. 4 shows the schematics of the analog micromirror arrays. The micromirrors that scan perpendicular to the array direction (array A) have been reported in [6], [8], and [13] and shown excellent stability in open-loop operations [9], [14]. Similar vertical comb drives are employed in the micromirrors with orthogonal scan direction (array B). The devices are fabricated using the SUMMiT-V surface-micromachining process provided by Sandia National Laboratories [20]. It has five polysilicon layers, including one nonreleasable interconnect layer and four structural layers. The first two structural polysilicon layers are laminated to form lower combs. The third polysilicon layer is patterned into upper combs. The chemical–mechanical planarization (CMP) process before the deposit of the third polysilicon layer provides a clear separation between the upper and lower combs. The planar geometry also allows the finger spacing to be reduced to 1 μm. The narrow gap spacing greatly increases the torque of the vertical comb actuators, which allows the mirror to operate at low voltages.

Fig. 5 shows the scanning electron microscope (SEM) images of both micromirrors. The vertical combs and springs are completely covered by the mirrors. Furthermore, by eliminating the guiding structure between mirrors, high fill factors are achieved: 97.5% for array A (156-μm mirror on 160-μm pitch) and 96.25% for array B (154-μm mirror on 160-μm pitch). The design rules of SUMMiT-V permit fill factors as high as 99.4%. In these devices, we have also extended the shielding electrode underneath the mirrors to increase the long-term stability. The area of exposed dielectric is minimized to avoid dielectric charging effect. Comb fingers near the edges of the mirrors are removed to minimize crosstalk between adjacent mirrors caused by the fringe field.

The scan angles of the micromirrors are measured using a noncontact interferometric surface profiler (WYKO). Fig. 6 shows the DC scan characteristics. The maximum mechanical

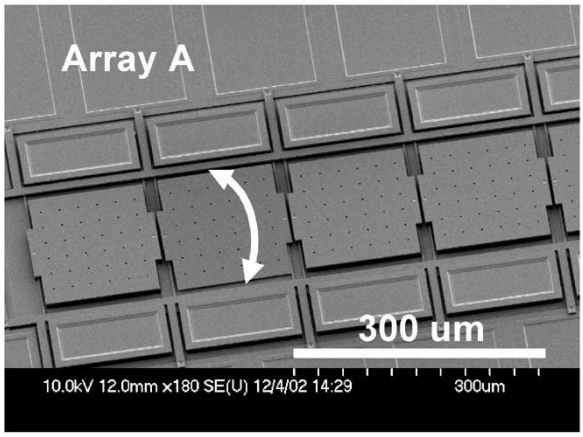

(a)

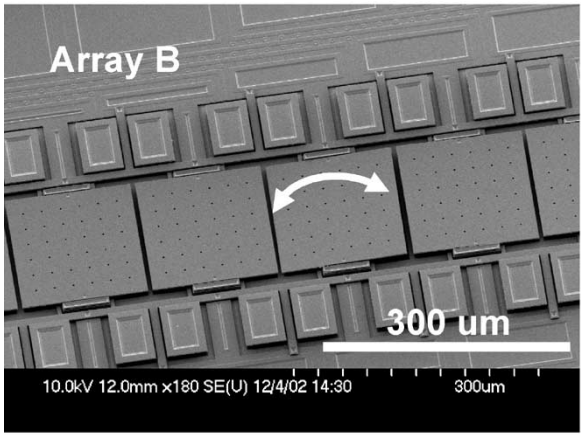

(b)

Fig. 5. SEM of micromirror arrays with (a) perpendicular and (b) parallel scan directions (in reference to the array direction).

scan angles are $\pm 5^\circ$ (7 V) and $\pm 6.3^\circ$ (7.5 V) for arrays A and B, respectively.

V. System Performance

A. $1 \times N^2$ WSS With 2-D Array of Discrete Collimators

We have constructed a prototype system using lenses with 15-cm focal length and 2-in aperture. A channel spacing of 75 GHz is attained with an 1100 grooves/mm grating. The Gaussian beam radius on the MEMS mirror (w_{MEMS}) is 30 μm. The number of wavelength channels is 15, which is limited by the number of mirrors in the array that can fit on the SUMMiT-V chip. The optical system can support up to 32 channels. It accommodates a 3×3 array of discrete fiber collimators at the input plane, which can be used as a 1×8 WSS with the input collimator located at the center of the array. The fiber-to-fiber insertion loss of the system is measured to be 6 ± 1 dB when the laser beam is coupled back to the input fiber collimator.

When the laser beam is switched to a fiber port right below the input collimator (i.e., vertical switching), the insertion loss is measured to be 8.6 dB. When switched to a diagonal port at one of the corners (i.e., diagonal switching), the insertion loss is 14 dB. Fig. 7 shows the spectral response at the input and output fibers. Diagonal switching and vertical switching are demonstrated with solid lines and dotted lines, respectively. The spectra are obtained using an amplified spontaneous emission (ASE) source. Ten of the 15 wavelength channels are shown in the plots. Switching at 1550 nm is clearly observed. The extinction ratio is 35 dB. The ripples at 1552.5 nm are due

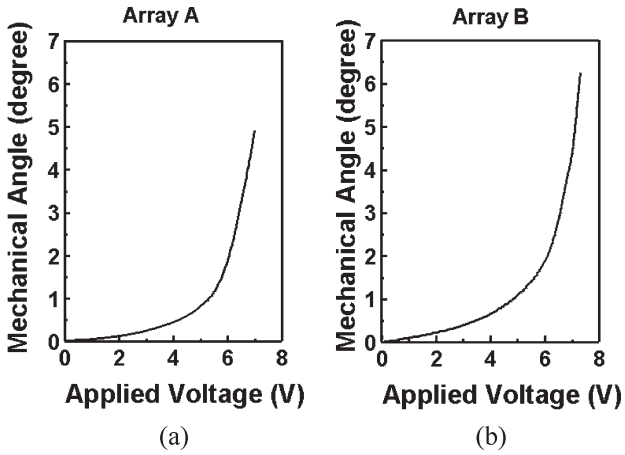

(a) (b)

Fig. 6. DC scan characteristics of the micromirrors with (a) perpendicular and (b) parallel scan directions.

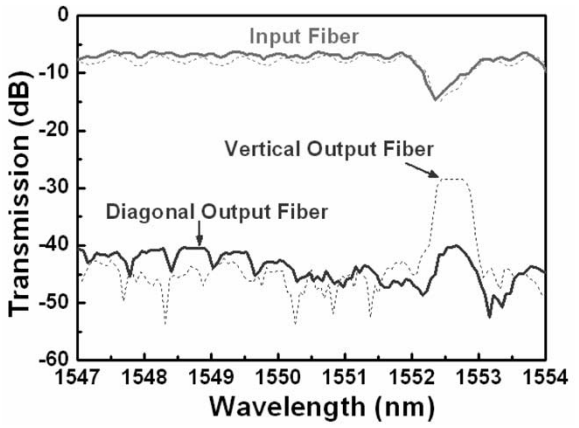

(a)

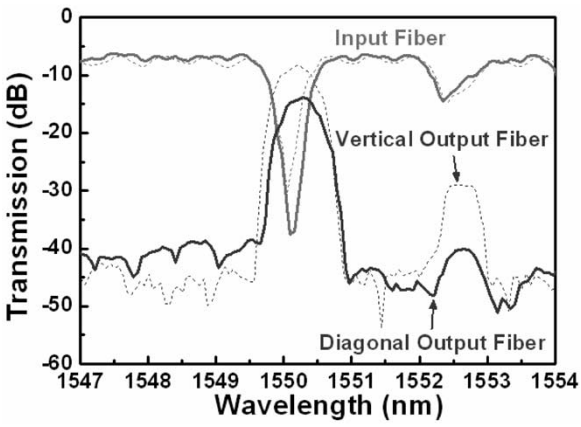

(b)

Fig. 7. Spectral response at the input and output fibers when (a) all the wavelength channels are coupled back to the input fiber and (b) the signal of 1550 nm is switched. The ripples around 1552.5 nm are due to a broken mirror. Diagonal switching and vertical switching are demonstrated with solid lines and dotted lines, respectively.

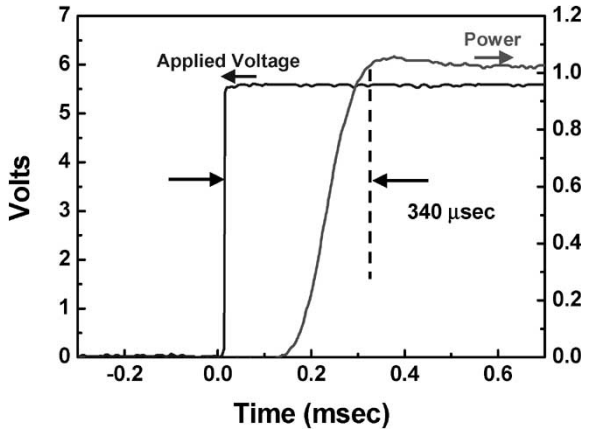

Fig. 8. Measured switching time of the wavelength-selective $1 \times N^2$ switch.

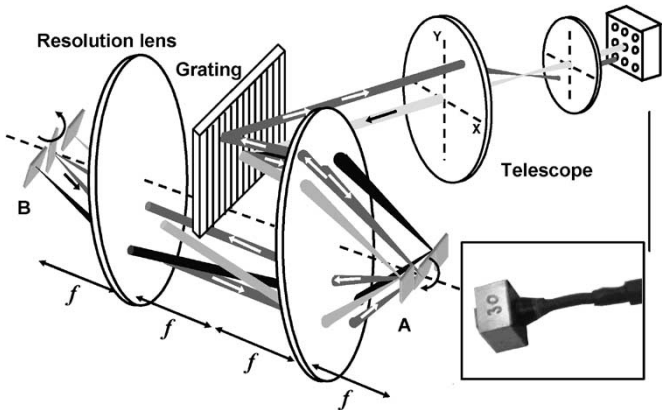

Fig. 9. Schematic setup of the $1 \times N^2$ WSS with a monolithic 2-D collimator array. The telescope is used to expand the beam size.

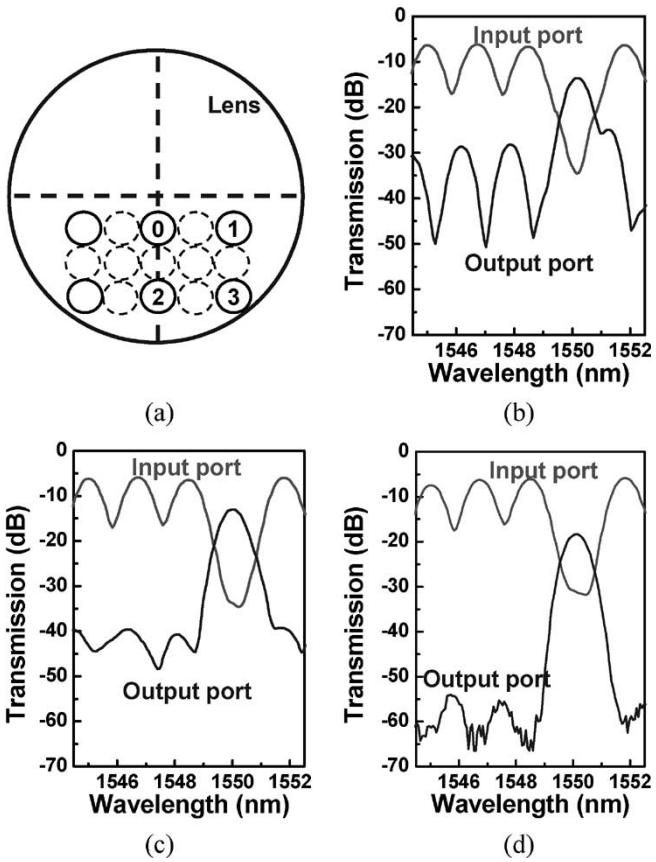

Fig. 10. (a) Cross-section of the $1 \times N^2$ WSS. Port 0 is the input, while the other ports are serving as the outputs. (b)–(d) Spectra when the 1550-nm wavelength channel is switched to ports 1, 2, and 3, respectively. Five wavelength channels are shown.

to a broken mirror in the array, which scatters light into the output fibers. The passband shape is deformed due to the mirror curvature and can be further improved by increasing the flatness of the micromirrors [21]. Fig. 8 shows the temporal response, which is characterized by switching the signal from the input port to the neighbor output port. The switching time is less than 340 μs.

B. $1 \times N^2$ *WSS With Monolithic 2-D Collimator Array*

The alignment of individual collimators is a cumbersome process. A monolithic 2-D fiber collimator array can overcome the above disadvantages. A commercial 6×6 fiber collimator array (purchased from Zygo TeraOptix) is used in our setup. The pitch of the array is 1 mm, with a beam radius of 125 μm. A $12\times$ telescope expands the optical beams before they are spatially dispersed by the grating, as illustrated in the schematic (Fig. 9). The picture of the collimator array is shown in the inset. The beam expander reduces the optical spot size on the MEMS mirror. A 600 grooves/mm grating and two lenses with 15-cm focal length and 2-in aperture are selected for our system. Six of the 36 (6×6) spatial channels are covered by the effective lens area after being imaged through the telescope beam expander. Therefore, it functions as a 1×5 WSS. The port count can be increased to 1×14 (3×5 ports covered) by improving the fill factor of the 2-D collimator array [dotted circles in Fig. 10(a)]. The microlens diameter-to-pitch ratio of our current collimator array is relatively low (50%). The Gaussian beam radius on the MEMS mirror (w_{MEMS}) is 46 μm.

Fig. 10(a) shows the cross-section of the $1 \times N^2$ WSS. Port 0 is the input, while the other ports are serving as the outputs. Fig. 10(b)–(d) shows the spectra when the 1550-nm wavelength channel is switched to ports 1, 2, and 3, respectively. The other wavelength channels are coupled back to the input port. Five of the 15 channels (200-GHz channel spacing) are shown. For the spectrum at the horizontal output port (1) [Fig. 10(b)], the -15-dB interchannel response below the signal level is due to coherent diffraction from the mirror edges [18], [19]. As predicted, such interchannel response is not observed at the vertical output port (2) [Fig. 10(c)]. The fiber-to-fiber insertion loss is measured to be 6 ± 1 dB when the laser beam is coupled back to the input fiber collimator. The effect of the mirror curvature on the passband shape is also observed in this configuration. Fig. 11 shows the temporal response when the light is switched from the input port to the neighbor output port. The switching time is less than 700 μs. This architecture with a monolithic 2-D collimator array exhibits a longer switching time. This is due to the fact that the angle difference between two adjacent physical ports is larger than that of the system using discrete collimators given the relatively low fill factor (50%) of the 2-D collimator array.

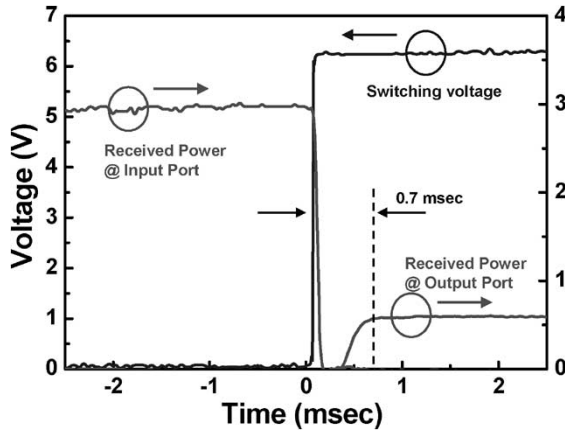

Fig. 11. Measured switching time of the wavelength-selective $1 \times N^2$ switch.

C. Discussion on the Port-Dependent Insertion Loss

Both configurations exhibit port-dependent insertion loss: 6–14 dB for the system with discrete collimators and 6–18 dB for the one using a monolithic 2-D collimator array. In both cases, the worst optical insertion loss is observed when the light is switched diagonally. The insertion loss variation across ports can be partially attributed to imperfect optical alignment. However, the aberration of the resolution lenses shall play a more decisive role in the port-dependent loss. The lenses used in our setups are the off-the-shelf achromatic doublet lenses obtained from Thorlabs Inc. Although achromatic doublet lenses perform better than singlet lenses in terms of mitigating aberration, they are still not as powerful as custom-made multiple-element lenses. The effect of spherical aberration on the port-dependent loss is illustrated in Fig. 12. Fig. 12(a) shows a $4-f$ imaging system with ideal lenses (no aberration). Assuming placing a point object on the left focal plane of the entire system, each emerging ray can be viewed as the reflected light beam from the MEMS mirror (dotted box) poised at a certain corresponding tilt angle. Based on geometric optics, in such a $4-f$ system using ideal lenses, all rays are to cross the point image located on the right focal plane. This means that in a $1 \times N^2$ WSS using ideal lenses, the optical beam focused on any mirror in the first array is always directed to the corresponding mirror in the second array, and vice versa, irrespective of the tilting angle of the mirrors. On the other hand, in a $4-f$ system with nonideal lenses (spherical aberration), split images occur along the optical axis as shown in Fig. 12(b). If a MEMS mirror is placed on the right focal plane, each ray hits the micromirror on a different spot, depending on the angle at which it emerges from the point object (i.e., scan-angle-dependent walk-off from the mirror center). Translating this concept into a $1 \times N^2$ WSS with nonideal resolution lenses, clipping loss by the micromirror in the second array is expected, depending on the rotation angle of the corresponding mirror in the first array, and vice versa. In the case of diagonally switching, beam walk-off occurs in both directions, leading to a relatively higher insertion loss.

VI. Conclusion

We report a novel high-port-count $1 \times N^2$ WSS using two cross-scanning one-axis analog micromirror arrays in a $4-f$ optical system. This exploits the use of the second dimension for accommodating the spatial ports, and overcomes the scaling limit by optical diffraction. The number of output ports is dramatically increased from N to N^2. Experimental results with both 2-D array of discrete collimators (1×8 WSS with 75-GHz channel spacing) and monolithic 2-D collimator array (1×5 WSS with 200-GHz channel spacing, scalable to 1×14) are successfully demonstrated. A fiber-to-fiber insertion loss of 6–18 dB and a switching time of < 700 μs have been achieved.

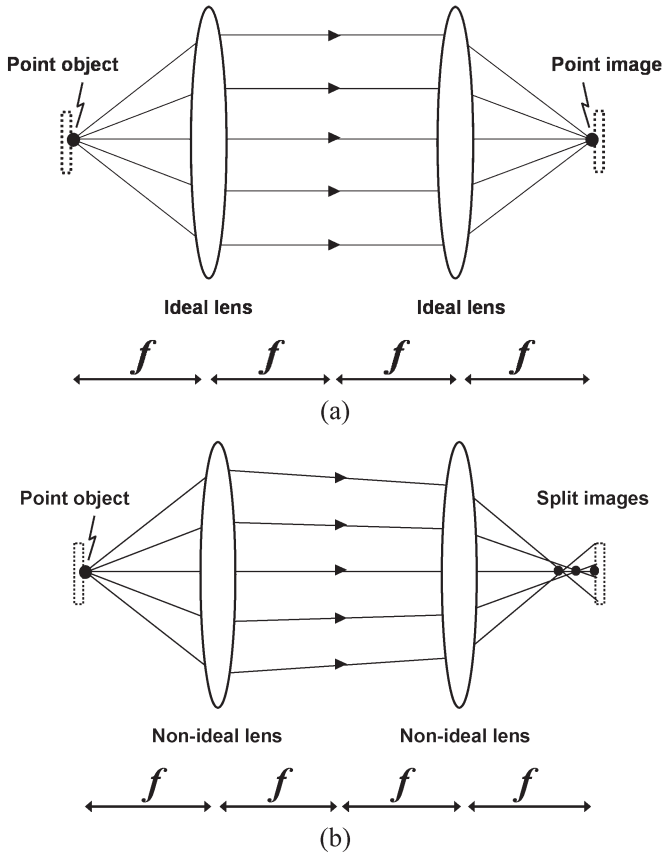

Fig. 12. Effect of spherical aberration in a $4-f$ imaging system. The dotted boxes are imaginary MEMS mirrors.

Acknowledgment

The authors would like to thank Prof. J. Ford of the University of California, San Diego, for helpful discussions, and M.-C. Lee, C.-H. Chi, and W. Piyawattanametha of University of California, Los Angeles (UCLA) for SEM images and technical assistance.

References

[1] L. Y. Lin, E. L. Goldstein, and R. W. Tkach, "Free-space micromachined optical switches for optical networking," *IEEE J. Sel. Topics Quantum Electron.: Special Issue on Microoptoelectro-Mechanical Systems (MOEMS)*, vol. 5, no. 1, pp. 4–9, Jan./Feb. 1999.

[2] A. Husain, "MEMS-based photonic switching in communications networks," in *Proc. Optical Fiber Communication (OFC)*, Anaheim, CA, 2001, pp. WX1-1–WX1-3.

[3] R. Ryf *et al.*, "1296-port MEMS transparent optical crossconnect with 2.07 Petabit/s switch capacity," in *Proc. Optical Fiber Communication (OFC)*, Anaheim, CA, 2001, pp. PD28-1–PD28-3.

[4] J. S. Patel and Y. Silberberg, "Liquid crystal and grating-based multiple-wavelength cross-connect switch," *IEEE Photon. Technol. Lett.*, vol. 7, no. 5, pp. 514–516, May 1995.
[5] J. E. Ford, V. A. Aksyuk, D. J. Bishop, and J. A. Walker, "Wavelength add-drop switching using tilting micromirrors," *J. Lightw. Technol.*, vol. 17, no. 5, pp. 904–911, May 1999.
[6] D. Hah, S. Huang, H. Nguyen, H. Chang, H. Toshiyoshi, and M. C. Wu, "A low voltage, large scan angle MEMS micromirror array with hidden vertical comb-drive actuators for WDM routers," in *Proc. Optical Fiber Communication (OFC)*, Anaheim, CA, 2002, pp. 92–93.
[7] D. M. Marom *et al.*, "Wavelength-selective 1×4 switch for 128 WDM channels at 50 GHz spacing," in *Proc. Optical Fiber Communication (OFC)*, Anaheim, CA, 2002, pp. FB7-1–FB7-3.
[8] D. Hah, S. Huang, H. Nguyen, H. Chang, J. C. Tsai, and M. C. Wu, "Low voltage MEMS analog micromirror arrays with hidden vertical comb-drive actuators," in *Proc. Solid-State Sensor, Actuator, and Microsystems Workshop*, Hilton Head Island, SC, Jun. 2002, pp. 11–14.
[9] S. Huang, J. C. Tsai, D. Hah, H. Toshiyoshi, and M. C. Wu, "Open-loop operation of MEMS WDM routers with analog micromirror array," in *Proc. IEEE/LEOS Optical MEMS Conf.*, Lugano, Switzerland, 2002, pp. 179–180.
[10] T. Ducellier *et al.*, "The MWS 1×4: A high performance wavelength switching building block," in *Proc. Eur. Conf. Optical Communication (ECOC)*, Copenhagen, Denmark, 2002. session 2.3.1.
[11] D. M. Marom *et al.*, "Wavelength selective 4×1 switch with high spectral efficiency, 10 dB dynamic equalization range and internal blocking capability," in *Proc. Eur. Conf. Optical Communication (ECOC)*, Rimini, Italy, 2003.
[12] ——, "64 channel 4×4 wavelength-selective cross-connect for 40 Gb/s channel rates with 10 Tb/s throughput capacity," in *Proc. Eur. Conf. Optical Communication (ECOC)*, Rimini, Italy, 2003, Paper We4.P.130.
[13] D. Hah, S. T. Y. Huang, J. C. Tsai, H. Toshiyoshi, and M. C. Wu, "Low-voltage, large-scan angle MEMS analog micromirror arrays with hidden vertical comb-drive actuators," *IEEE J. Microelectromech. Syst.*, vol. 13, no. 2, pp. 279–289, Apr. 2004.
[14] J. C. Tsai, S. Huang, D. Hah, H. Toshiyoshi, and M. C. Wu, "Open-loop operation of MEMS-based $1 \times N$ wavelength-selective switch with long-term stability and repeatability," *IEEE Photon. Technol. Lett.*, vol. 16, no. 4, pp. 1041–1043, Apr. 2004.
[15] J. C. Tsai, S. Huang, D. Hah, and M. C. Wu, "Wavelength-selective $1 \times N^2$ switches with two-dimensional input/output fiber arrays," in *Proc. Conf. Lasers and Electro-Optics (CLEO)*, Baltimore, MD, 2003. Paper CTuQ4.
[16] ——, "Analog micromirror arrays with orthogonal scanning directions for wavelength-selective $1 \times N^2$ switches," in *Proc. Transducers*, Boston, MA, 2003, pp. 1776–1779.
[17] ——, "$1 \times N^2$ wavelength-selective switch with telescope-magnified 2D input/output fiber collimator array," in *Proc. IEEE/LEOS Optical MEMS Conf*, Waikoloa, HI, 2003, pp. 45–46.
[18] D. M. Marom and S. H. Oh, "Filter-shape dependence on attenuation mechanism in channelized dynamic spectral equalizers," in *Proc. Lasers and Electro-Optics Society (LEOS)*, Glasgow, Scotland, 2002, pp. 416–417.
[19] S. H. Oh and D. M. Marom, "Attenuation mechanism effect on filter shape in channelized dynamic spectral equalizers," *Appl. Opt.*, vol. 43, no. 1, pp. 127–131, Jan. 2004.
[20] [Online]. Available: http://www.sandia.gov/mstc/technologies/micromachines/tech-info/technologies/summit5.html
[21] D. M. Marom *et al.*, "Effect of mirror curvature in MEMS micro-mirror based wavelength-selective switches," in *Proc. IEEE/LEOS Annu. Meeting*, Tucson, AZ, 2003, pp. 305–306.

Jui-che Tsai received the B.S. degree in electrical engineering and the M.S. degree in electro-optical engineering from the National Taiwan University (NTU), Taipei, Taiwan, R.O.C., in 1997 and 1999, respectively, and the Ph.D. degree in electrical engineering from the University of California, Los Angeles (UCLA), in 2005.

Between 1999 and 2001, he served in the military as a Second Lieutenant. Before joining the faculty of NTU, he was a postdoctoral researcher with the Department of Electrical Engineering and Computer Sciences, and Berkeley Sensor and Actuator Center (BSAC), University of California, Berkeley. He is currently an Assistant Professor at the Graduate Institute of Electro-Optical Engineering and Department of Electrical Engineering, NTU. His research interests include optical microelectromechanical systems (MEMS), optical fiber communication, and biophotonics.

Sophia Ting-Yu Huang received the B.S. degree (*summa cum laude*) in electrical engineering from the University of California, Los Angeles, in 2000, the B.A. degree (*magna cum laude*) in management-engineering from Claremont McKenna College, Claremont, CA, in 2000, and the M.S. degree in electrical engineering with focus in photonics from the University of California, Los Angeles, in 2002.

Since 2002, she has been working in Los Angeles and New York City.

Dooyoung Hah received the M.S. and Ph.D. degrees in electrical engineering from the Korea Advanced Institute of Science and Technology (KAIST), Daejon, Korea, in 1996 and 2000, respectively. His Ph.D. dissertation topic was a low-voltage RF microelectromechanical systems (MEMS) switch.

Before joining the Louisiana State University (LSU), Baton Rouge, he was with the University of California, Los Angeles, as a Postdoctoral Researcher from 2000 to 2001 and as a Staff Research Associate from 2004 to 2005, and at the Electronics and Telecommunications Research Institute (ETRI), Korea, as a Senior member of the Research Staff from 2002 to 2004. He is currently an Assistant Professor of Electrical and Computer Engineering at the LSU. He has authored and coauthored over 40 publications including journal papers and international conference proceedings. He also holds five U.S. and six Korea patents. His research interests include MOEMS, RF MEMS, MEMS for biomedical applications, microactuators, sensors, and nanotechnology.

Dr. Hah was the third place winner at the student paper competition at the 2000 IEEE MTT-s.

Ming C. Wu (S'82–M'83–SM'00–F'02) received the B.S. degree from the National Taiwan University, Taipei, Taiwan, R.O.C., in 1983 and the M.S. and Ph.D. degrees from the University of California (UC), Berkeley, in 1985 and 1988, respectively, all in electrical engineering.

Before joining the faculty of UC Berkeley, he was a member of Technical Staff at AT&T Bell Laboratories, Murray Hill, NJ, from 1988 to 1992, and a Professor of Electrical Engineering at UCLA from 1993 to 2004. He also held the position of Director of Nanoelectronics Research Facility and Vice Chair for Industrial Relations during his tenure at UCLA. In 1997, he co-founded OMM in San Diego, CA, to commercialize MEMS optical switches. He is currently a Professor of Electrical Engineering and Computer Sciences at the University of California, Berkeley, and the Co-Director of Berkeley Sensor and Actuator Center (BSAC). His research interests include optical microelectromechanical systems (MEMS), optoelectronics, and biophotonics. He has published over 400 papers, contributed five book chapters, and holds 11 U.S. patents.

Dr. Wu is a David and Lucile Packard Foundation Fellow (1992–1997). He was the founding Co-Chair of the IEEE Lasers and Electro-Optics Society (LEOS) Summer Topical Meeting on Optical MEMS (1996), the predecessor of the IEEE/LEOS International Conference on Optical MEMS. He has also served in the program committees of many technical conferences, including MEMS, OFC, CLEO, LEOS, MWP, IEDM, DRC, ISSCC, and as Guest Editor of two special issues of the IEEE JOURNAL ON OPTICAL MEMS.